# ALTAIR'S OBLATENESS AND ROTATION VELOCITY FROM LONG-BASELINE INTERFEROMETRY

Gerard T. van Belle[1]

Jet Propulsion Laboratory, California Institute of Technology, Pasadena, CA 91109; gerard@huey.jpl.nasa.gov

David R. Ciardi

Department of Astronomy, University of Florida, Gainesville, FL, 32611; ciardi@astro.ufl.edu

Robert R. Thompson

Jet Propulsion Laboratory, California Institute of Technology, Pasadena, CA 91109, and Department of Physics & Astronomy, University of Wyoming, Laramie, Wyoming 82071; thompson@huey.jpl.nasa.gov

Rachel L. Akeson

Infrared Processing and Analysis Center, California Institute of Technology, Pasadena, CA 91125; akeson@huey.jpl.nasa.gov

AND

Elizabeth A. Lada

Department of Astronomy, University of Florida, Gainesville, FL, 32611; lada@astro.ufl.edu

*Received 2000 November 26; accepted 2001 June 5*

## ABSTRACT

We present infrared interferometric angular size measurements for the A7IV-V star Altair that indicate a noncircular projected disk brightness distribution. Given the known rapid rotation of this star, we model the data as arising from an elongated rigid atmosphere. To first order, an ellipse may be fitted to our interferometric diameter measurements, with major and minor axes of $2a = 3.461 \pm 0.038$ mas and $2b = 3.037 \pm 0.069$ mas, respectively, for a difference of $424 \pm 79$ $\mu$as between $2a$ and $2b$, and with an axial ratio of $a/b = 1.140 \pm 0.029$. Assuming that the apparent oblateness of the photosphere is due to the star's rapid rotation, a more rigorous evaluation of the observation data in the context of a rigidly rotating Roche model shows that an estimate of $v \sin i = 210 \pm 13$ km s$^{-1}$ can be derived that is independent of spectroscopic techniques. Also derived are values for the mean effective temperature and the mean linear radius, and an observational constraint upon the relationship between rotation velocity and stellar inclination is established. Altair is the first main-sequence star for which direct observations of an oblate photosphere have been reported and the first star for which $v \sin i$ has been established from observations of the star's photospheric geometry.

*Subject headings:* stars: fundamental parameters — stars: individual (Altair) — infrared: stars — techniques: interferometric

*On-line materials:* color figures

## 1. INTRODUCTION

The star Altair ($\alpha$ Aql, HR 7557, HD 187642) is a well-studied object, being the 12th brightest star in the sky and one of the 50 nearest stars to the Sun (Allen 1973; Perryman et al. 1997). It is an A7IV-V main-sequence star (Johnson & Morgan 1953) and is known to be a rapid rotator, with an atmosphere that has been extensively modeled (e.g., Gouttebroze et al. 1999). The measurements of the star's apparent rotational velocity ($v \sin i$) range from 190 km s$^{-1}$ (Carpenter, Slettbak, & Sonneborn 1984) up to 250 km s$^{-1}$ (Stoeckley 1968), depending upon the spectral lines used in the investigation. These values of $v \sin i$ are a substantial fraction of the star's estimated critical velocity of 430 km s$^{-1}$ (Gray 1976), where centripetal acceleration at the stellar equator exceeds gravitational acceleration.

Stellar rotation has been measured observationally for almost a century, beginning with Schlesinger (1909, 1911). Models of rotating stars have explored the impact of rotation upon both stellar effective temperature (Slettebak 1949) and stellar shape (Collins 1963, 1965; Collins & Harrington 1966). Recently models have begun to incorporate the effects of differential rotation as a function of stellar latitude (Zahn 1992). Rotation impacts important observable pa-

rameters such as photometry (Collins & Smith 1985) and surface brightness distributions, as originally shown by von Zeipel (1924a, 1924b), and rotation has nontrivial implications upon stellar evolution, as explored in the various papers by, among others, Claret and Maeder (see Martin & Claret 1996; Claret 2000; Maeder 1997, 2000).

Up until now, however, virtually all observational evidence underpinning the theoretical models has been based upon velocities inferred from spectroscopic line broadening. While this technique is both well understood and well developed, it is susceptible to confusion with other influences upon spectral line widths, such as various turbulence mechanisms and latitude dependencies of line emission (see Carpenter et al. 1984 and references therein). An independent means by which to determine the parameters governing the structure of centrifugally-distorted stars would be welcome.

The 3 mas angular diameter of Altair was observed 30 yr ago by Hanbury Brown and his colleagues with the Intensity Interferometer at Narrabri (Hanbury Brown et al. 1967, 1974). While the authors comment upon the possibility and observational implications of this star being rotationally flattened in their first paper, they did not explicitly solve for this possibility owing to data insufficient to constrain an oblate model (J. Davis 2000, private communication). As such, Jordahl (1972) examines the Intensity Interferometer

---

[1] For preprints, please contact gerard@huey.jpl.nasa.gov.

results in the context of apparent disk brightness distribution resulting from stellar rotation theory, although this is done from the perspective of its effects upon the average angular diameter.

Herein we report the determination of the overall diameter and projected shape of Altair upon the sky from near-infrared, long-baseline interferometric measurements taken with the Palomar Testbed Interferometer (PTI). PTI is an 85 and 110 m $H$- and $K$-band (1.6 and 2.2 $\mu$m) interferometer located at Palomar Observatory and is described in detail in Colavita et al. (1999). PTI has a minimum $K$-band fringe spacing of $\approx 4.3$ mas at the sky position of Altair, making this particular object readily resolvable.

*Direct observation* of the stellar disk can provide unique insight into basic stellar parameters. The measured angular size in conjunction with the bolometric flux and distance yields constraints on parameters such as effective temperature and linear radii, both of which remain quantities poorly established empirically for virtually all stars. Upon fitting a family of rotating models for the projected stellar photosphere upon the sky, we further demonstrate that a unique value for $v \sin i$ may be derived from the interferometric data.

The PTI observations that produced these results are discussed in § 2, detailing source selection and observation. In § 3 the procedures used in establishing the stellar parameters for the stars observed are discussed: the parameters include spectral type, bolometric flux, major and minor axial angular sizes, effective temperature and linear radius. Finally, in § 4 we demonstrate that an apparent rotational velocity and other observational parameters may be derived from Altair's oblateness by fitting the data with the appropriate family of Roche models.

## 2. OBSERVATIONS

The interferometric observable used for these measurements is the fringe contrast or visibility (squared) of an observed brightness distribution on the sky. Normalized in the interval [0:1], a single star exhibits monochromatic visibility modulus in a uniform disk model given by

$$V^2 = \left[ \frac{2J_1(\theta_{\mathrm{UD}} \pi B \lambda^{-1})}{\theta_{\mathrm{UD}} \pi B \lambda^{-1}} \right]^2 , \quad (1)$$

where $J_1$ is the first-order Bessel function, $B$ is the projected baseline vector magnitude at the star position, $\theta_{\mathrm{UD}}$ is the apparent angular diameter of the star, and $\lambda$ is the wavelength of the interferometric observation. The $V^2$ observables used in our Altair study are the synthetic wideband $V^2$'s, given by an incoherent signal-to-noise (SNR) weighted average $V^2$ of the five narrowband channels in the PTI spectrometer (Colavita 1999). In a similar fashion, incoherent SNR-weighted average bandpasses $\lambda$ were determined from the raw data. The PTI $H$ and $K$ wavebands are excellent matches to the CIT photometric system (Colavita et al.

1999; Elias et al. 1982, 1983). Separate calibrations and fits to the narrowband and synthetic wideband $V^2$ data sets yield statistically consistent results, with the synthetic wideband data exhibiting superior SNR. Consequently, we will present only the results from the synthetic wideband data.

Altair was observed in conjunction with Vega and objects in our calibrator list by PTI at 2.2 $\mu$m on seven nights between 1999 May 25 and 2000 July 27. For three of the nights, PTI's north-west 85 m baseline was utilized; for the remaining four nights, the north-south 110 m baseline was used; the results from each baseline are consistent across all nights. Altair, along with calibration objects, was observed multiple times during each of these nights, and each observation, or scan, was approximately 130 s long. For each scan we computed a mean $V^2$-value from the scan data, and the error in the $V^2$ estimate from the rms internal scatter (Colavita 1999). Altair was always observed in combination with one or two calibration sources within 3° on the sky. For our study we have used two main-sequence stars as calibration objects: HD 187691 (F8V) and HD 187923 (G0V). The stars are expected to be nearly unresolved by the interferometer with predicted angular sizes less than 0.75 mas; expected angular size and error were based upon a blackbody radiator angular size inferred from available broadband photometry, particularly in the near-infrared.[2] Clearly, many stars deviate significantly from blackbody behavior (see van Belle et al. 1999); however, the main-sequence stars of F and G spectral type selected as primary calibrators should not deviate sharply from blackbody behavior. These objects were additionally selected to be slow apparent rotators, with $v \sin i < 20$ km s$^{-1}$ (Uesugi & Fukuda 1982). Table 1 lists the relevant physical parameters for the calibration objects.

The calibration of Altair $V^2$ data is performed by estimating the interferometer system visibility ($V^2_{\mathrm{sys}}$) using calibration sources with model angular diameters and then normalizing the raw Altair visibility by $V^2_{\mathrm{sys}}$ to estimate the $V^2$ measured by an ideal interferometer at that epoch (Mozurkewich et al. 1991; Boden et al. 1998). Uncertainties in the system visibility and the calibrated target visibility are inferred from internal scatter among the data in a scan and standard error-propagation calculations. More detail on PTI's target & calibrator selection, data reduction (van Belle et al. 1999) and technical aspects (Colavita et al. 1999) is available in the literature. Calibrating our Altair data set with respect to the two calibration objects listed in Table 1 results in a total of 27 calibrated scans on Altair over seven nights in 1999 and 2000. Calibrating our two calibration objects against each other produced no evidence of systematics, with both objects delivering reduced $V^2$'s $\approx 1$, as expected. Our calibrated synthetic wideband $V^2$ measurements are summarized in Table 2, along with derived values as discussed in § 3. Altair's $V^2$ measurements are plotted

[2] See D. Y. Gezari, P. S. Pitts, & M. Schmitz 1996, Catalog of Infrared Observations, version 4, at http://ircatalog.gsfc.nasa.gov/cio.

TABLE 1

CALIBRATION SOURCES

| Source | $\theta_{\mathrm{EST}}$ (mas) | Distance from Altair (deg) | Spectral Type | $v \sin i$ (km s$^{-1}$) | Notes |
|---|---|---|---|---|---|
| HD 187691...... | $0.72 \pm 0.10$ | 1.6 | F8V | 5 | Primary calibrator |
| HD 187923...... | $0.51 \pm 0.10$ | 2.8 | G0V | 15 | |

TABLE 2

The Observed Data for Altair

| MJD | Wavelength[a] (μm) | Normalized $V^2$ | Hour Angle (hr) | Projected Baseline (m) | Position Angle[b] (deg) | Uniform Disk Angle Size (mas) |
|---|---|---|---|---|---|---|
| 51323.41...... | 2.204 | 0.164 ± 0.010 | −1.57 | 106.58 | 237 | 3.368 ± 0.048 |
| 51323.43...... | 2.204 | 0.174 ± 0.013 | −1.12 | 104.78 | 240 | 3.379 ± 0.058 |
| 51323.46...... | 2.205 | 0.195 ± 0.014 | −0.40 | 101.54 | 245 | 3.390 ± 0.063 |
| 51323.48...... | 2.202 | 0.207 ± 0.015 | 0.05 | 99.56 | 249 | 3.400 ± 0.065 |
| 51729.34...... | 2.242 | 0.192 ± 0.007 | −0.59 | 102.43 | 243 | 3.428 ± 0.032 |
| 51729.37...... | 2.241 | 0.229 ± 0.010 | 0.12 | 99.22 | 249 | 3.374 ± 0.044 |
| 51729.39...... | 2.240 | 0.241 ± 0.009 | 0.64 | 97.17 | 254 | 3.389 ± 0.040 |
| 51730.35...... | 2.248 | 0.217 ± 0.030 | −0.38 | 101.47 | 245 | 3.360 ± 0.124 |
| 51730.36...... | 2.249 | 0.257 ± 0.043 | −0.10 | 100.22 | 247 | 3.233 ± 0.167 |
| 51731.33...... | 2.247 | 0.174 ± 0.023 | −0.65 | 102.70 | 243 | 3.512 ± 0.105 |
| 51731.35...... | 2.246 | 0.197 ± 0.030 | −0.37 | 101.41 | 245 | 3.449 ± 0.133 |
| 51731.35...... | 2.246 | 0.197 ± 0.021 | −0.34 | 101.27 | 245 | 3.451 ± 0.094 |
| 51731.36...... | 2.248 | 0.210 ± 0.036 | −0.09 | 100.16 | 247 | 3.434 ± 0.155 |
| 51749.29...... | 2.232 | 0.462 ± 0.062 | −0.59 | 86.46 | 195 | 2.875 ± 0.213 |
| 51749.30...... | 2.232 | 0.473 ± 0.044 | −0.35 | 86.19 | 196 | 2.851 ± 0.166 |
| 51749.35...... | 2.233 | 0.428 ± 0.043 | 0.82 | 80.62 | 200 | 3.229 ± 0.174 |
| 51749.36...... | 2.233 | 0.422 ± 0.042 | 1.07 | 78.54 | 201 | 3.339 ± 0.175 |
| 51751.23...... | 2.228 | 0.418 ± 0.016 | −1.77 | 83.24 | 193 | 3.163 ± 0.065 |
| 51751.24...... | 2.225 | 0.415 ± 0.021 | −1.59 | 84.22 | 193 | 3.131 ± 0.082 |
| 51751.26...... | 2.232 | 0.419 ± 0.017 | −1.20 | 85.73 | 194 | 3.070 ± 0.065 |
| 51751.33...... | 2.228 | 0.449 ± 0.024 | 0.61 | 82.12 | 199 | 3.081 ± 0.093 |
| 51751.34...... | 2.229 | 0.437 ± 0.025 | 0.79 | 80.81 | 199 | 3.181 ± 0.099 |
| 51752.22...... | 2.226 | 0.440 ± 0.018 | −2.01 | 81.70 | 193 | 3.130 ± 0.073 |
| 51752.23...... | 2.227 | 0.422 ± 0.015 | −1.84 | 82.84 | 193 | 3.160 ± 0.059 |
| 51752.25...... | 2.228 | 0.400 ± 0.021 | −1.24 | 85.63 | 194 | 3.142 ± 0.084 |
| 51752.26...... | 2.229 | 0.397 ± 0.021 | −1.07 | 86.05 | 194 | 3.143 ± 0.083 |
| 51752.28...... | 2.227 | 0.376 ± 0.022 | −0.65 | 86.47 | 195 | 3.208 ± 0.086 |

[a] SNR-weighted average wavelength of the narrowband channels used to construct the SNR-weighted average $V^2$

[b] P.A. is east of north.

versus spatial frequency in Figure 1, and the uniform disk angular size versus projected baseline angle on the sky are plotted for Altair and Vega in Figure 2.

### 3. STELLAR PARAMETERS

#### 3.1. Spectral Type and Bolometric Flux
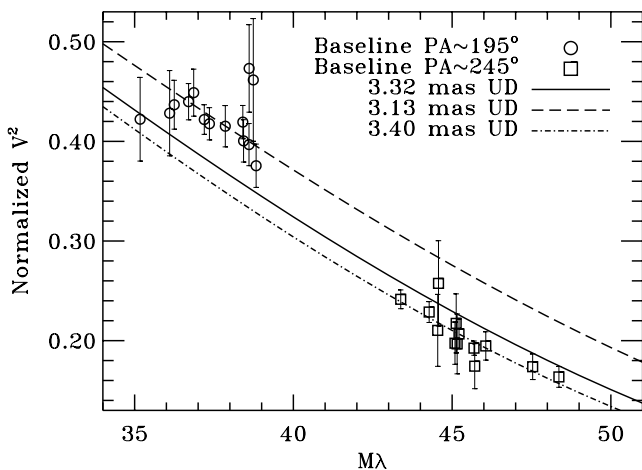
Although varying spectral subtypes and luminosity



FIG. 1.—Visibility data for Altair. The visibility points at ≈37 Mλ correspond to a baseline projection angle of ≈195° with a 3.137 ± 0.025 mas uniform disk angular size, and the visibility points at ≈45 Mλ correspond to a baseline projection angle of ≈245° with a 3.400 ± 0.018 mas angular size. These two baseline projections result from the north-south and north-west baselines of PTI. A single 3.22 mas disk fit to all of the points clearly is inadequate to fully characterize the data.

classes are given for Altair, its spectral type is generally accepted to be A7IV-V (Johnson & Morgan 1953; Gliese & Jahreiss 1991). Bolometric flux was taken from the calibration of Alonso, Arribas, & Martinez-Roger (1994), who calculate it to be $F_{bol} = 1217 \pm 46 \times 10^8$ ergs cm$^{-2}$ s$^{-1}$.

#### 3.2. Apparent Stellar Disk

Once a normalized value for $V^2$ has been obtained, the simplest interpretation is to fit a uniform disk angular size as presented in equation (1). Altair, with $\theta_{UD} < 4$ mas, falls well within the monotonic region of the uniform disk function for the 110 m baseline of PTI at 2.2 μm. The normalized values for $V^2$ for each observation are listed in Table 2, with their associated observation Julian Date, wavelength, hour angle, projected interferometer baseline and rotation angle, and uniform disk angular size.

Fitting a single global value of $\theta_{UD}$ to the $V^2$ data ensemble results in a mean uniform disk size of 3.317 ± 0.013 mas with a reduced $\chi^2$ per degree of freedom (dof) of $\chi^2/$dof = 3.71. However, as seen in Figure 1, this fit systematically underestimates $V^2$ near 37 Mλ and overestimates near 45 Mλ. The smaller spatial frequencies correspond to PTI's north-west baseline, which is rotated approximately 50° from PTI's north-south baseline, which was used to obtain the data at larger spatial frequencies. This discrepancy can be addressed by relaxing the assumption of spherical symmetry and including the position angle of the observations in the fit. A spherical gaseous star will deform when rotating; such a shape projected onto the sky will appear, to first order, as an ellipse. For given physical situations, the true geometry of a rotating star will depart from that of an
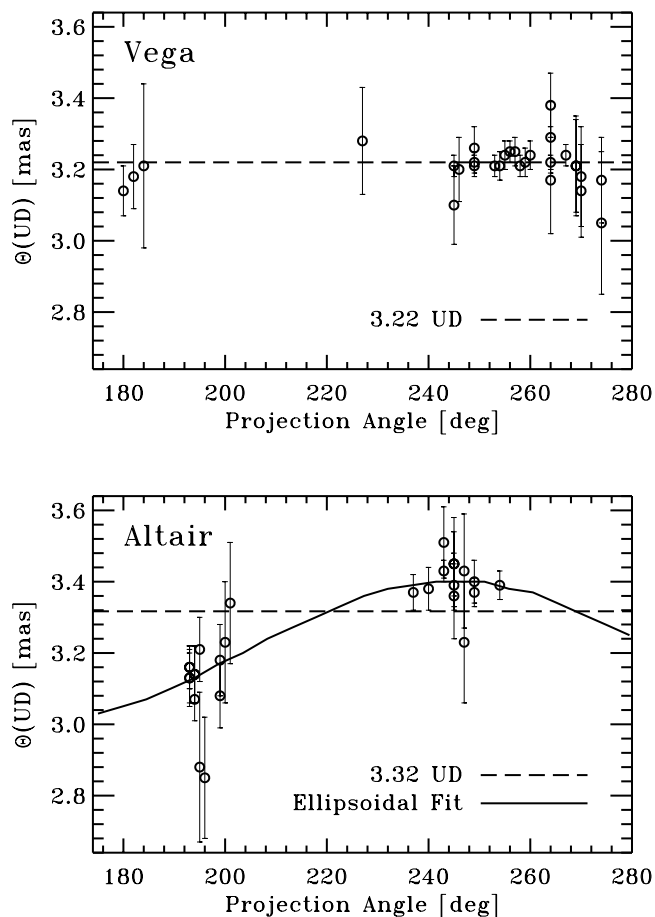
FIG. 2.—Uniform disk sizes as a function of baseline projection angle for Altair and Vega

ellipsoid at the 5%-6% level, and we will return to this in a much more precise fashion in § 4. However, such a fit is useful as a metric to initially establish the position angle dependence of our angular size data. Using the basic equation for an ellipse,

$$\theta_{\mathrm{UD}}(\alpha) = \frac{2ab}{\sqrt{a^2\sin^2(\alpha - \alpha_0) + b^2\cos^2(\alpha - \alpha_0)}}, \quad (2)$$

we may solve for a projection angle–dependent angular size, where $2a$, $2b$ are the major and minor axes of the ellipse on the sky in mas, respectively, and $\alpha_0$ is the orientation angle of the ellipse on the sky, where $\alpha_0 = 0$ corresponds to the minor axis pointing to the north on the sky. Fitting equation (2) to the data in Table 2, we find that $2a = 3.403 \pm 0.031$ mas, $2b = 2.986 \pm 0.066$ mas, and $\alpha_0 = 25 \pm 9°$ with $\chi^2/\mathrm{dof} = 0.53$. An illustration of these fits and the data is seen in Figure 3.

In contrast to this finding is contemporaneous data taken of Vega. Data for both stars and their respective calibrators were taken within an hour of each other during observing runs in 1999 and 2000. Vega is best fitted by a $3.223 \pm 0.008$ mas circular disk, with $\chi^2/\mathrm{dof} = 0.45$; no regular deviations in the Vega $V^2$ data are seen similar to the Altair data. An ellipsoidal fit to the observed Vega visibilities results in an axial ratio of $a/b = 1.024 \pm 0.032$ with $\chi^2/\mathrm{dof} = 0.38$, which is of negligible significance statistically. The Vega observations are discussed in detail in Ciardi et al. (2001). The uniform disk sizes versus baseline projection angle for both
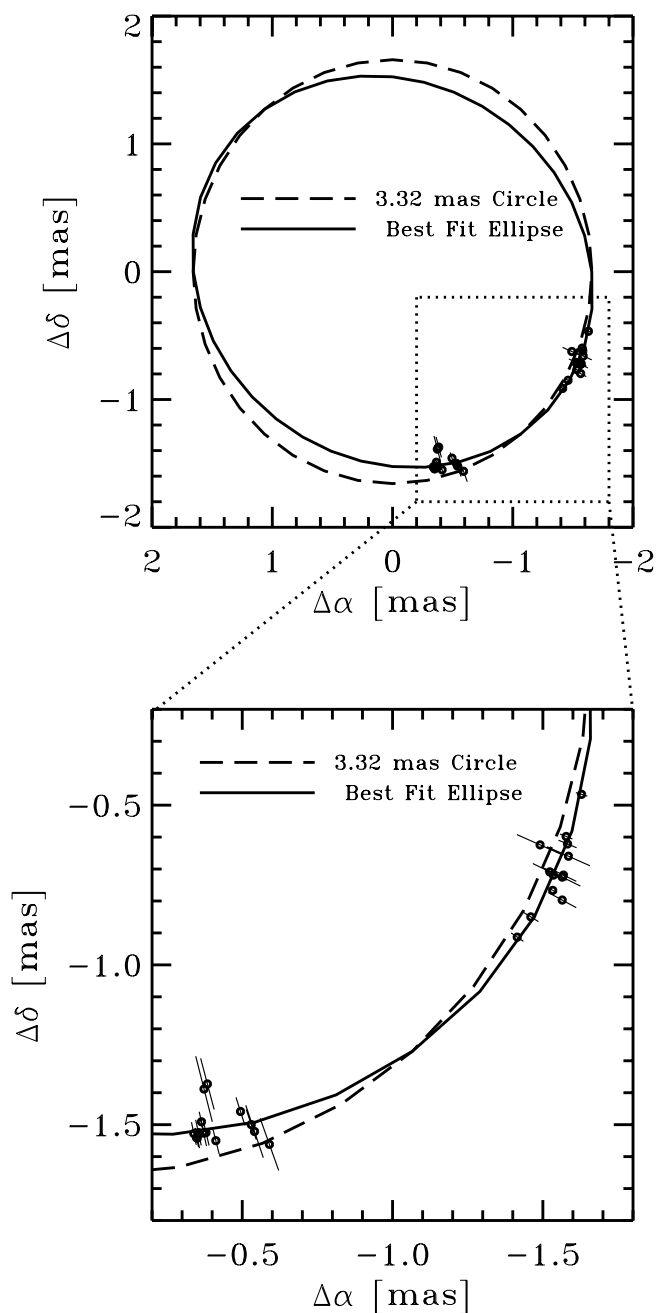


FIG. 3.—Data points along the limb of Altair. The data subsets at the two mean position angles each contain 13–14 data points.

Vega and Altair can be seen in Figure 2. This figure shows that, in contrast to our Vega data, Altair's $V^2$ data are poorly fitted by a single uniform disk model. Our surprise at this result was somewhat mitigated by corroborating preliminary indications from the Navy Prototype Optical Interferometer (NPOI) that their Altair results also exhibit sky position angle dependencies (T. E. Nordgren 2000, private communication).

Other potential causes for Altair's departure from circularly symmetric $V^2$ data may be ruled out. If Altair were either a true or line-of-sight binary star, our interpretation of the $V^2$ variations with baseline length and position angle would be incorrect. However, Altair is indicated to be a single star from astrometric investigations (Gatewood & de Jonge 1995; Perryman, Gatewood, & Wagman 1997) in

contrast to earlier indications to the contrary (Russell et al. 1978). This result is consistent with the recent *HST* NICMOS investigation of the star indicating no nearby late-type or substellar companions (Kuchner & Brown 2000), who rule out the possibility of companions with $\Delta J \leq 10$ further than $1\overset{''}{.}4$ from the primary, which corresponds to 3.3 AU at the distance of Altair. The possibility of a line-of-sight companion may be further investigated given the fact that Altair is known to be a star with a large proper motion of roughly $0\overset{''}{.}65$ yr$^{-1}$ (Perryman et al. 1997). Examining the 40-50 year old plates from the first Palomar Sky Survey indicates that Altair's $\approx 30''$ of proper motion did not move it to within $5''$ of any objects brighter than $V \approx 10$ magnitude. Assuming an average color of $V - K = 3$, we can infer no line-of-sight companions with $K < 7$. As such, the Altair/companion ratio would be $\Delta K > 6$. As demonstrated in Boden et al. (1998), PTI is largely insensitive to companions with $\Delta K > 4$. Thus, the possibility of the $V^2$ variations arising from binarity is strongly ruled out.

We also consider other potential deviations of the apparent disk of Altair from that of a uniform brightness distribution. The presence of limb darkening will affect a star's observed visibility curve and potentially bias our results. For a slowly rotating star, this effect is independent of stellar latitude and is observed to be an increased dimming of the stellar disk from center to limb. For Altair's relatively compact stellar atmosphere, the general effect of compositional limb darkening upon the observed visibility curve out to the first null is negligible at 2.2 $\mu$m. Linear limb-darkening for a nonrotating Altair (log $g = 4.0$, $T_{\mathrm{eff}} = 7750$ K; Claret, Diaz-Cordoves, & Gimenez 1995) is $u(2.2 \ \mu\mathrm{m}) = 0.203$ for the linear limb-darkening characterization $I(\mu) = I(1)[1 - u(1 - \mu)]$, where $u$ is the linear limb-darkening coefficient, $\mu = \cos \theta$ describes the angle between the line of sight and the emergent flux, and $I(1)$ is the monochromatic specific intensity at the center of the disk. Computing a visibility curve from this center-to-limb brightness profile and comparing it to that of a uniform disk indicates that angular sizes for slowly rotating stars derived under the assumption of a uniform disk fit will be undersized by a factor of 1.017. These brightness profiles and their resultant visibility functions are seen in Figure 4.

However, for a rapidly rotating star, this phenomenon takes on an additional latitude dependence, often referred to in the literature as gravity-darkening or gravity-brightening (e.g., Claret 2000). As first shown by von Zeipel (1924a), the polar zones of stars distorted by rapid rotation will be hotter than their equatorial zones, because the poles are closer to the center of the star. The consequential non-uniform flux distribution over the stellar surface affects a star's visibility curve. However, as is the case with a slowly rotating star, the impact is for the visibility curve to depart from that of a uniform disk primarily after the first zero, as also seen in Figure 4. We computed visibility curves for a center-to-limb brightness profile as above, but with an additional 25% brightness at the poles covering 20% of the star's surface, at a variety of stellar orientations relative to the interferometer baseline. These parameters are consistent with Altair models found in Jordahl (1972), which for $i = 60°$ range in temperature from $T = 7100$ K to $T = 9300$; between the temperature extremums, flux at 2.2 $\mu$m will increase by a factor of 1.5. Comparison of the resultant visibility curves indicated that the uniform disk angular
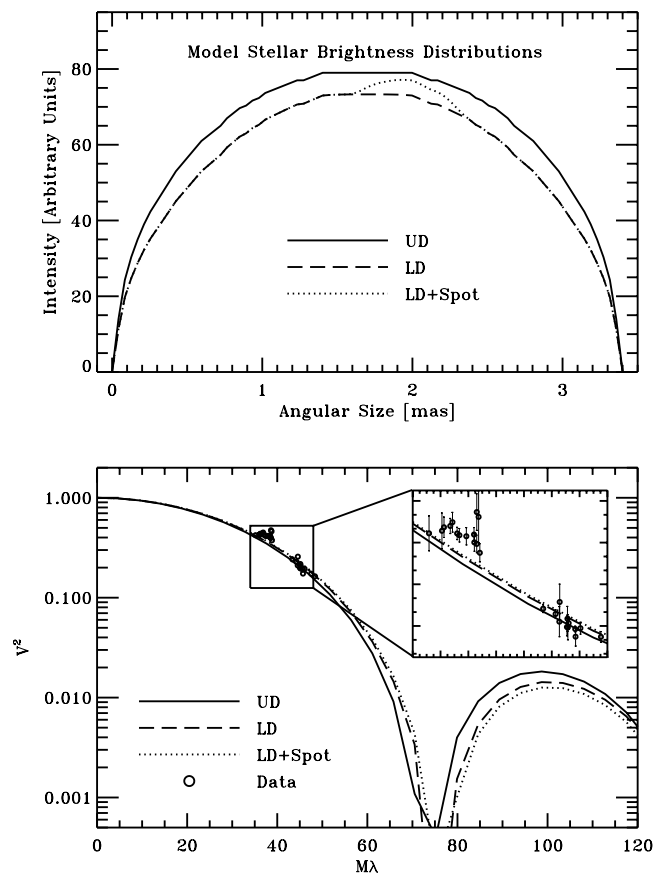


FIG. 4.—Representative stellar model used in calculating the effect of both limb darkening and gravity darkening upon the resultant visibility curve. The upper plot is the one-dimensional strip brightness for a uniform disk (*dotted line*), limb-darkened disk (*solid line*), and a limb-darkened disk with a spot that has a 25% brightness enhancement and is 20% of the stellar disk size (*dashed line*). Below, the resultant $V^2$ curves are plotted. A uniform disk fit to the spotted model, randomly oriented upon the sky, will result in a systematic size estimate that is a factor of $1.017 \pm 0.006$ too small.

sizes derived for a rapidly rotating star like Altair will deviate from the true angular sizes by factors of 1.011 to 1.029, depending upon star orientation.

Figure 4 shows the strip brightness distribution and resultant visibility curve for a uniform disk, a $u = 0.203$ limb-darkened disk, and a limb-darkened disk with a random bright spot. A Monte Carlo simulation of the various visibility curves from random orientations of such a star indicated that angular sizes derived using uniform disk fits would underestimate the star's true size by $1.017 \pm 0.006$. Similar simulations of limb-darkened stars with larger (25%) or brighter (50%) spots show underestimates of $1.020 \pm 0.013$ and $1.021 \pm 0.017$, respectively, once again depending upon the star's orientation upon the sky. The overall scaling implied by these surface brightness distributions do not account for the "step" in $V^2$ data seen in Figure 1, and the scale of the discontinuity in the data is approximately 3.5 times larger than the limb-darkening scaling implied from our strip brightness distribution modeling.

On average, the size underestimate due to limb- or gravity-darkening is a marginal adjustment and is included in our data reduction process merely for the sake of completeness; the multiplicative factor of $1.017 \pm 0.006$ is suffi-

TABLE 3
BASIC PARAMETERS DERIVED FROM THE DATA AND ASSEMBLED FROM THE LITERATURE

| Parameter | Value | Units | Reference |
|---|---|---|---|
| Given | | | |
| Spectral type ........... | A7IV-V | | Johnson & Morgan 1953 |
| Parallax ................. | 194.45 ± 0.94 | mas | Perryman et al. 1997 |
| $\theta$ (0.5 $\mu$m) .............. | 2.98 ± 0.14 | mas | Hanbury Brown et al. 1974 |
| $F_{BOL}$ .................... | 1217 ± 46 | $10^8$ ergs cm$^2$ s$^{-1}$ | Alonso et al. 1994 |
| $M$ ....................... | 1.80 | $M_\odot$ | Malagnini & Morossi 1990 |
| Ellipsoidal fit | | | |
| $a_R$ ....................... | 3.461 ± 0.038 | mas | This work |
| $b_R$ ....................... | 3.037 ± 0.069 | mas | This work |
| Position angle .......... | −25 ± 9 | deg | This work |
| $R_a$ ....................... | 1.915 ± 0.023 | $R_\odot$ | This work |
| $R_b$ ....................... | 1.681 ± 0.039 | $R_\odot$ | This work |
| Roche models | | | |
| $R_e(\omega)$ ................... | 1.8868 ± 0.0066 | $R_\odot$ | This work |
| $\alpha$ ......................... | −21.6 ± 6.2 | deg | This work |
| $v \sin i$.................... | 210 ± 13 | km s$^{-1}$ | This work |
| Additional derived values | | | |
| $a_R/b_R$ .................... | 1.140 ± 0.029 | | This work |
| $a_R - b_R$ ................. | 424 ± 79 | $\mu$as | This work |
| $\overline{\theta}_R$ ........................ | 3.242 ± 0.041 | mas | This work |
| $\overline{R}$........................ | 1.794 ± 0.023 | $R_\odot$ | This work |
| $v_{crit}$ ....................... | 426 ± 12 | km s$^{-1}$ | This work |

cient to convert our $\theta_{UD}$ sizes to Rosseland (photospheric) angular sizes, $\theta_R$. Our resultant major and minor axes are $a_R = 3.461 \pm 0.038$ mas, $b_R = 3.037 \pm 0.069$ mas. For an equivalent circular area projected upon the sky, we have $\overline{\theta}_R = 3.242 \pm 0.041$. The axial ratio $a_R/b_R$ is $1.140 \pm 0.029$, and the difference between the axes is $a_R - b_R = 424 \pm 79$ $\mu$as.

### 3.3. Effective Temperature

Although we may compute a single effective temperature from our data on Altair, it must be stressed that this will be nothing more than a mathematical construct derived from geometrical considerations for the purposes of characterizing the gross properties of the star. The stellar effective temperature $T_{eff}$ is defined in terms of the star's luminosity and radius by $L = 4\pi\sigma R^2 T_{eff}^4$. Rewriting this equation in terms of angular diameter and bolometric flux $F_{bol}$, a value of $T_{eff}$ was calculated from the flux and mean Rosseland diameter $\overline{\theta}_R$ using

$$T_{eff} = 2341 \times \left(\frac{F_{bol}}{\overline{\theta}_R^2}\right)^{1/4} = 2341 \times \left(\frac{F_{bol}}{a_R b_R}\right)^{1/4}, \quad (3)$$

the units of $F_{bol}$ are $10^{-8}$ ergs cm$^2$ s, and $\overline{\theta}_R$, $a_R$, $b_R$ are in mas. The error in $T_{eff}$ is calculated from the usual propagation of errors applied to equation (3). The resultant mean $T_{eff}$ for Altair is determined here to be $7680 \pm 90$ K. This single value for effective temperature is solely derived from geometric considerations and is probably an inadequate true characterization of the stellar surface. As mentioned in § 3.2, Altair models that account for gravity-darkening effects (Jordahl 1972) show temperatures that range with stellar latitude from 7100 to 9300 K or more, depending upon rotation speed.

Previous estimates of Altair's $T_{eff}$ range from $8250 \pm 180$ K as determined by intensity interferometry (Hanbury Brown et al. 1967), to 8080 K from modeling (Malagnini & Morossi 1990), while Blackwell, Petford, & Shallis (1979)

infer 7588 K from the infrared flux method (IRFM). The discrepancy between our value and Hanbury Brown et al.'s is attributable to two effects: recent (and presumably more accurate) bolometric flux estimates and our angular size (and hence, derived $T_{eff}$) is larger. The discrepancy in $\overline{\theta}_R$ is most likely due to the effect of either limb darkening, which is greater (and harder to estimate) at visible wavelengths (as used by the Intensity Interferometer), or limited sampling. For values of $T_{eff}$ derived using just the angular size as indicated from the major axis $a_R$, the inferred temperatures would be 250 K too low; using just $b_R$, 250 K too high.

A larger implication of this result is the potential inaccuracy of effective temperatures derived from angular diameters at single projections across the disks of rotationally distorted stars. This effect can be as significant as limb darkening in ascertaining a star's $T_{eff}$, an effect which is expected to be routinely considered in all studies of stellar effective temperature.

### 3.4. Linear Radius

If we take the parallax for Altair, $\pi = 194 \pm 0.94$ mas, as determined by *Hipparcos* (Perryman et al. 1997), and combine it with a mean angular diameter of $\overline{\theta}_R = 3.242 \pm 0.041$ mas obtained in § 3.2, we obtain an average photospheric radius $R = 1.794 \pm 0.023$ $R_\odot$. (Following the unfortunately contradictory conventions in the literature, we shall present angular sizes in terms of diameters and linear sizes in terms of radii.) However, as discussed in § 3.2, the exact radius of Altair is not best fitted by a single number. From the apparent major and minor axes, we may quantify the radii of the star at the extreme latitudes. At the equator, the stellar radius should simply be equal to the projected major axis, $R_a = 1.915 \pm 0.023$ $R_\odot$. At the poles, the radius will be less than or equal to the projected minor axis, $R_b = 1.681 \pm 0.039$ $R_\odot$. Given the unknown inclination of the star relative to our line of sight, it is likely the star's radius at the poles is even smaller.

As with Altair's effective temperature, the mean linear size we derive is in good agreement with $R = 1.82 \ R_\odot$ derived from the infrared flux method (Shallis & Blackwell 1980). From their parallax measurement in conjunction with the Hanbury Brown et al. (1967) value for $\theta_R$, Gatewood & de Jonge (1995) estimate $R = 1.63 \pm 0.08 \ R_\odot$. A summary of Altair's stellar parameters is presented in Table 3.

## 4. DISCUSSION

The key to understanding the peculiar diameter results for Altair lies in its rapid rotation. Different values for $v \sin i$ for the star have been derived from spectral line broadening profiles, depending upon the spectral line used: Carpenter et al. (1984) derive $190 \pm 38$ km s$^{-1}$ from *IUE* UV data; Freire Ferrero et al. (1978) derive 220 km s$^{-1}$ from the visible Ca II lines; Stoeckley (1968) derives $250 \pm 10$ km s$^{-1}$ by observing visible Mg I and Ca II lines.

In contrast to these values, the observed rotational velocity of Vega is roughly a factor of 10 lower, at less than 20 km s$^{-1}$ (Freire Ferrero et al. 1983), which is consistent with its apparent lack of oblateness. While Vega has been reported to be a rapid rotator, this inference has been made in conjunction with the deduction that it is very nearly pole-on (Gulliver, Hill, & Adelman 1994) with $i = 5°–6°$, an orientation which would present the star to the interferometer as nearly circular upon the sky. As discussed in § 3.2 and in Ciardi et al. (2001), our data from PTI indicating circular symmetry for the disk of Vega are consistent with this conclusion.

We may more precisely investigate the rotational distortion of the photosphere of a star. The force of centripetal acceleration at the equator, resulting from the rotation, offsets the effect of gravitation owing to the mass of the star. Under the conditions of hydrostatic equilibrium, uniform rotation, and a point mass gravitational potential, we may derive the equatorial rotational velocity, assuming we view the star at an inclination angle $i$. As developed in the work by Collins (1963, 1965) and presented in Jordahl (1972), the equation of shape for such a star under rotation may be written as

$$\frac{GM}{R_p(\omega)} = \frac{GM}{R(\theta, \omega)} + \frac{1}{2} \omega^2 R(\theta, \omega)^2 \sin^2 \theta \qquad (4)$$

or

$$1 = \frac{1}{r(\theta)} + \frac{4}{27} u^2 r(\theta, u)^2 \sin^2 \theta , \qquad (5)$$

with substitutions for the normalized radius,

$$r(\theta, \omega) = \frac{R(\theta, \omega)}{R_p(\omega)} , \qquad (6)$$

and the dimensionless rotational speed $u$, as defined by

$$\omega^2 = u^2 \frac{8}{27} \frac{GM}{R_p^3(\omega)} , \qquad (7)$$

where $R(\theta, \omega)$ is the stellar radius at colatitude $\theta$ for a star of mass $M$ rotating at angular velocity $\omega$, $R_p(\omega)$ is the polar radius for that star, and $G$ is the gravitational constant. As is appropriate in utilizing their mathematical constructs, we also adopted the coordinate system that is graphically illustrated in Collins (1965) and Jordahl (1972). Clearly there are more recent and/or more complicated models than this simple Roche model, but for the purposes of this analysis, we shall consider it sufficient. Solving for the cubic equation (5) trigonometrically, we can arrive at an expression for the colatitude-dependent stellar radius at a rotation speed $u$:

$$r(\theta, u) = \frac{3}{u \sin \theta} \cos \left[ \frac{\cos^{-1} (-u \sin \theta) + 4\pi}{3} \right]. \qquad (8)$$

For the following computations, we used values of 1.8 $M_\odot$ for the mass of Altair and a parallax of $\pi = 194.45 \pm 0.94$ mas. Such a Roche model is applicable for a rigidly rotating star, which is consistent with a fully radiative stellar atmosphere. Fortunately, for the case of A-type main-sequence star Altair, this is a reasonable expectation. It is worth noting that, in contrast to our elliptical approximation in § 3.2, this approach exactly solves for the expected shape of the stellar limb.

To interpret our radius data, we began by constructing models of Altair based upon rotation $u$ and polar radius $R_p(\omega)$, which are sufficient to map the entire surface as a function of stellar colatitude and longitude. Model surfaces were constructed for the full star at intervals of 0°.5 in both colatitude and longitude across the whole volume. These models were then mapped onto the sky and matched to the observational data through the use of two additional angular parameters, inclination $i$ and on-sky rotational orientation $\alpha$ at steps of 0°.1 along the entire circumference of the stellar limb.

Thus, for a given set of four randomized free parameters $\{u, R_p(\omega), i, \alpha\}$, a 300,000 point volume surface was generated, projected upon the sky, and fitted to the angular diameter data, and a $\chi^2$/dof was calculated. A multidimensional optimization code was then utilized to derive the best $\{u, R_p(\omega), i, \alpha\}$ solution from the random starting point, a process that took typically 500 iterations (Press et al. 1992). An exhaustive search of the rotating star parameter space was used to explore the $\chi^2$/dof space. Furthermore, a static grid of $\{u, i\}$ values was explored for optimal $\{R_p(\omega), \alpha\}$ values to ensure that no local minima were trapping the optimization code. The grid consisted of 1,000 points spread uniformly over the space enclosed by $u = [0 : 1]$, $i = [0 : 90]$ and was run multiple times with random $\{R_p(\omega), \alpha\}$ seed values, to ensure full mapping of the resultant $\{u, i\}$ $\chi^2$/dof surface. Trial runs of the $\chi^2$/dof minimization technique using artificial data sets from synthetic stars were able to fully recover the original four parameter characterization for the original synthetic star. The model data sets covered a wider range of position angles, from 5° to 175° in 5° steps, but with angular size errors comparable to the Altair data set, which on average are 2.3% per measurement. The $\chi^2$/dof surface resulting from the Altair data set is plotted in Figure 5, where $\{R_p(\omega), \alpha\}$ are optimized for minimum $\chi^2$/dof for a given pair of $\{u, i\}$ coordinates.

There is a noticeable trough in the $\chi^2$/dof surface obtained via this technique, running from $u = 0.77$ at $i = 90°$ (corresponding to viewing the star equator-on) to $u = 1.00$ at $i = 31°.9$. Any inclination less than 31°.9 is physically inconsistent with our observed data. Unfortunately, there is no global minima that is differentiated from the other best fits in a statistically significant manner. Instead, we fitted for the trough in $\{u, i\}$ $\chi^2$/dof space, mapping the family of models enclosed by $+1$ of $\chi^2$/dof that describe the

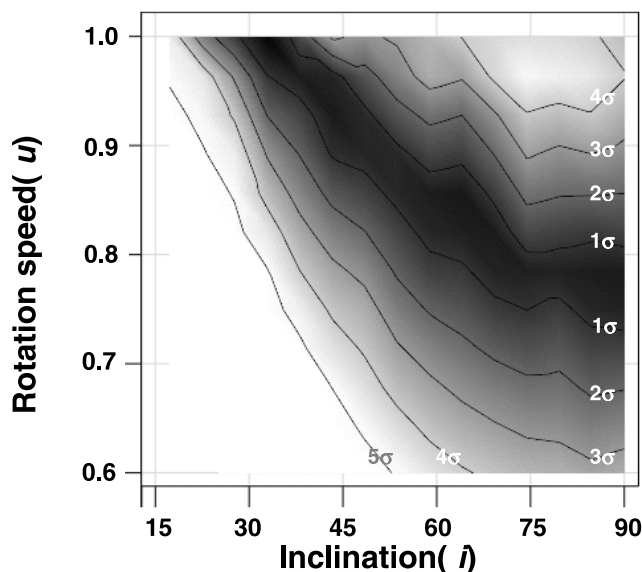FIG. 5.—$\chi^2$/dof surface for Altair as a function of rotation $u$ and inclination $i$. [*See the electronic edition of the Journal for a color version of this figure.*]



FIG. 6.—Example three-dimensional model of Altair projected onto the sky ($u = 0.82$, $i = 70$), showing the fit of the PTI data to the limb of the stellar photosphere. Units are in meters at the distance of Altair. [*See the electronic edition of the Journal for a color version of this figure.*]

dependency of rotation $u$ upon inclination $i$:

$$u = 4.961 \times 10^{-5}(90 - i)^2 + 1.116 \times 10^{-3}(90 - i) + 0.762$$

$$. \tag{9}$$

From each member of this family of models, derived values for angular velocity $\omega$, equatorial radius $R_e(\omega)$, equatorial velocity $v_e$, and apparent rotation velocity $v \sin i$ may be derived. An interesting aspect of this family of models is that they present uniform values for $v \sin i$, $R_e(\omega)$ and $\alpha$. Taking the ensemble of solutions found in the trough and averaging the result, we find that $v \sin i = 210 \pm 13$ km s$^{-1}$. The preferred values for $R_e(\omega)$ and $\alpha$ are $1.8868 \pm 0.0066$ $R_\odot$ and $-21.6 \pm 6\overset{\circ}{.}2$ east of north for the pole, respectively, which are consistent with the values derived in § 3.2 for the ellipsoidal approximation. A illustration of a $\{u = 0.82, i = 70°\}$ potential solution for our data is given in Figure 6. Examining predicted equatorial radii from the family of models, we are able to establish a critical rotation velocity of

$$v_{\text{crit}} = \omega_c R_e(\omega_c) = \sqrt{\frac{GM}{R_e(\omega_c)^3}} R_e(\omega_c) = 426 \pm 12 \text{ km s}^{-1} ,$$

$$\tag{10}$$

given our constant equatorial radius and assuming a 10% error on Altair's mass. This value is consistent with the value of 430 km s$^{-1}$ from Gray (1976).

An improvement to this technique would be to incorporate latitude dependent limb- and gravity-darkening, derived from a latitude-dependent temperature profile and projected onto the sky, resulting in a relationship between baseline projection angle and the limb-darkening parameter $\mu$. Such an effort, however, is beyond the scope of this initial investigation into the observational appearance of rotational distorted photospheres. A variant of this approach has already been employed in the visible by Jordahl (1972), using the average angular size data of Hanbury Brown et al. (1974). In the near-infrared, as illustrated in § 3.2, we expect this to be a much smaller effect than in the visible, at the $\approx 1\%$ level,
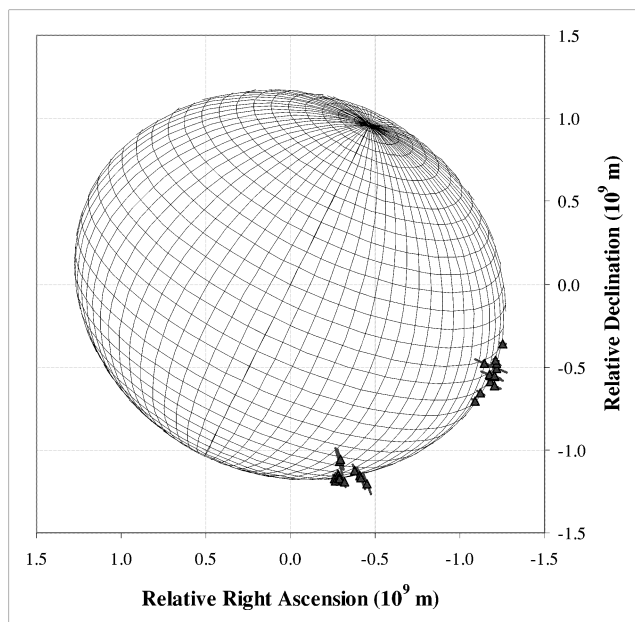
which is at a level much smaller than our typical angular size errors. A potential next step in the development of this technique would be to combine multiwavelength observations, potentially from multiple interferometers, to fit a ensemble of stellar models that features latitude-dependent temperatures.

Our derived value for $v \sin i$ is in good agreement with spectroscopically determined values, as presented in § 4. The dominant source of error in our technique is primarily located in the angular size data and secondarily in the mass estimate. The linear sizes are well constrained by the *Hipparcos* parallax, which has only a 0.4% quoted error, and dominated by the angular size error estimates of $\approx 2.3\%$.

Conversely, we may take a measured value for $v \sin i$ in conjunction with our values for stellar radius and attempt to infer the mass of the star. Unfortunately, this approach is unduly sensitive to errors in both the rotational velocity and measures of the stellar shape. For example, if we were to take $v \sin i$ for Altair to be 220 km s$^{-1}$ with a 10% error (see Freire Ferrero et al. 1995 and references therein), we measure the mass of this A7IV-V star to be $M = 1.74 \pm 0.49$ $M_\odot$. Substantial improvement in this measurement will be challenging: 1% values for polar, equatorial radii and $v \sin i$ still return only an 11% mass. A 1% mass from this technique requires 0.1% values for radii and rotational velocity, which appears currently highly challenging for both interferometry and spectroscopy.

Our measurements represent the first ever direct asymmetry observations for a main-sequence star. We emphasize here that all other stars with reported asymmetries are either Mira variables or supergiant stars (see Lattanzi et al. 1997; Monnier, Tuthill, & Danchi 1999). Previous work indicates that the radii of the Mira and supergiant stars are hundreds of $R_\odot$ (Haniff, Scholz, & Tuthill 1995; van Belle et al. 1996, 1999); equation (4) indicates a carbon star such as V Hya with $v \sin i \approx 14$ (Barnbaum, Morris, & Kahane 1995) and $R \approx 400$ $R_\odot$ (van Belle et al. 1997) should exhibit

an oblateness of $a/b \approx 1.11$. While this is remarkable in itself, it is perhaps an unsurprising expectation for these stars with extended atmospheres; in contrast to that is our finding of asymmetry for the relatively compact atmosphere of Altair. We are not aware of any other observations of luminosity class V or IV–V stars that indicate convincing departure from circularly symmetric brightness distributions.

Recent studies of Altair's polarization (Piirola 1977; Tinbergen 1982) have indicated no statistically significant degree of polarization; as such, there is no comparison to be made between the apparent axes of the stellar photosphere and the polarization orientation.

## 5. CONCLUSIONS

We have measured the apparent oblateness of Altair's disk upon the sky and inferred its rotational velocity. This interferometric measurement of $v \sin i$ is independent of spectroscopic and photometric means that have characterized all previous rotational velocity measurement techniques. Furthermore, we have demonstrated a technique that, with sufficient data sampling around a stellar limb, has the potential to recover the inclination of rapidly rotating stars.

A simple examination of the rotational velocity catalog collated by Bernacca & Perinotto (1973) indicates there are over 70 known bright ($V < 4$) main-sequence stars in the northern hemisphere that are rapid rotators with $v \sin i >$ 200 km s$^{-1}$; examination of bright ($V < 8$) evolved objects in de Medeiros & Mayor (1999) that have $v \sin i >$ 15 km s$^{-1}$ indicates there are over 70 potential targets as well. Objects that fit these criteria should exhibit apparent flattening of their disks at the $\approx 10\%$ level. Clearly there are plenty of opportunities to implement this technique with the upcoming generation of long-baseline optical and infrared interferometers such as CHARA, NPOI, Keck, and VLTI, which all have multiple baselines allowing the required stellar disk projection measurements to be made in much shorter observing times. Our PTI follow-up observing campaign of $\alpha$ Leo and other rapidly rotating stars already has initial results that support this promising line of research.

For almost a century, the three basic methods for measuring axial rotation of stars have been line profile analysis, photometric modulation of starlight due to dark or bright areas on a rotating star, and radial velocity curve distortions in eclipsing binary systems (Slettebak 1985); of these, line profile analysis has been the most widely used. To these three methods, we add this fourth interferometric approach, which may have particular utility in servicing stars out of the reach of the other three methods. As noted in Gray (1976), spectroscopic determination of $v \sin i$ for rapidly rotating main-sequence stars from spectral lines is made difficult by line broadening; similarly, spectroscopic determination of $v \sin i$ for highly evolved objects is nontrival owing to density of features in their spectra (see Kahane, Maizels, & Jura 1988; Barnbaum et al. 1995). Not only is the value we have derived above in agreement with the velocities derived from various spectral lines, it is an independent check of $v \sin i$ values derived from spectroscopic or photometric means for rotationally flattened stars.

REFERENCES

Allen, C. W. 1973, Astrophysical Quantites (3d ed.; London: Athlone Press)
Alonso, A., Arribas, S., & Martinez-Roger, C. 1994, A&A, 282, 684
Barnbaum, C., Morris, M., & Kahane, C. 1995, ApJ, 450, 862
Bernacca, P. L., & & Perinotto, M. 1973, A Catalogue of Stellar Rotational Velocieties (Padova: Cleup)
Blackwell, D. E., Petford, A. D., & Shallis, M. J. 1979, A&A, 82, 249
Boden, A. F., et al. 1998, ApJ, 504, L39
Carpenter, K. G., Slettebak, A., & Sonneborn, G. 1984, ApJ, 286, 741
Ciardi, D. R., van Belle, G. T., Akeson, R. L., Thompson, R. R., Lada, E. A., & Howell, S. B. 2001, ApJ, in press
Claret, A. 2000, A&A, 359, 289
Claret, A., Diaz-Cordoves, J., & Gimenez, A. 1995, A&AS, 114, 247
Colavita, M. M. 1999, PASP, 111, 111
Colavita, M. M., et al. 1999, ApJ, 510, 505
Collins, G. W., II. 1963, ApJ, 138, 1134
———. 1965, ApJ, 142, 265
Collins, G. W., II., & Harrington, J. P. 1966, ApJ, 146, 152
Collins, G. W., II, & Smith, R. C. 1985, MNRAS, 213, 519
de Medeiros, J. R., & Mayor, M. 1999, A&AS, 139, 433
Elias, J., Frogel, J., Hyland, A., & Jones, T. 1983, AJ, 88, 1027
Elias, J., Frogel, J., Matthews, K., & Neugebauer, G. 1982, AJ, 87, 1029
Freire Ferrero, R., Gouttebroze, P., Catalano, S., Marilli, E., Bruhwweiler, F., Kondo, Y., van der Hucht, K., & Talavera, A. 1983, ApJ, 439, 1011
———. 1995, ApJ, 439, 1011

Freire Ferrero, R., Praderie, F., Czarny, J., & Felenbok, P. 1978, A&A, 61, 785
Gatewood, G., & de Jonge, J. K. 1995, ApJ, 450, 364
Gliese, W., & Jahreiss, H. 1991, Preliminary Version of the Third Catalog of Nearby Stars (Heidelberg: Rechen-Institut)
Gouttebroze, P., Freire Ferrero, R., Marilli, E., & Catalano, S. 1999, A&A, 348, 198
Gray, D. F. 1976, The Observation and Analysis of Stellar Photospheres (New York: Wiley-Interscience)
Gulliver, A. F., Hill, G., & Adelman, S. J. 1994, ApJ, 429, L81
Kahane, C., Maizels, C., & Jura, M. 1988, ApJ, 328, L25
Kuchner, M. J., & Brown, M. E. 2000, PASP, 112, 827
Hanbury Brown, R., Davis, J., & Allen, L. R. 1974, MNRAS, 167, 121
Hanbury Brown, R., Davis, J., Allen, L. R., & Rome, J. M. 1967, MNRAS, 137, 393
Haniff, C. A., Scholz, M., & Tuthill, P. G. 1995, MNRAS, 276, 640
Johnson, H. L., & Morgan, W. W. 1953, ApJ, 117, 313
Jordahl, P. R. 1972, Ph.D. thesis, Univ. Texas, Austin
Lattanzi, M. G., Munari, U., Whitelock, P. A., & Feast, M. W. 1997, ApJ, 485, 328
Maeder, A. 1997, A&A, 321, 134
———. 2000, NewA Rev., 44, 291
Malagnini, M. L., & Morossi, C. 1990, A&AS, 85, 1015
Martin, E. L., & Claret, A. 1996, A&A, 306, 408
Monnier, J. D., Tuthill, P. G., & Danchi, W. C. 1999, ApJ, 525, L97
Mozurkewich, D., et al. 1991, AJ, 101, 2207
Perryman, M. A. C., et al. 1997, A&A, 323, 49

Piirola, V. 1977, A&AS, 30, 213
Press, W. H., Teukolsky, S. A., Vetterling, W. T., & Flannery, B. P. 1992, Numerical Receipes in C (Port Chester: Cambridge Univ. Press)
Russell, J. L., Gatewood, G. D., & Wagman, N. E. 1978, AJ, 83, 1455
Schlesinger, F. 1909, Publ. Allegheny Obs., 1, 134
———. 1911, MNRAS, 71, 719
Shallis, M. J., & Blackwell, D. E. 1980, A&A, 81, 336
Slettebak, A. 1949, ApJ, 110, 498
———. 1985, in Calibration of Fundamental Stellar Quantities (Dordrecht: Reidel), 163
Stoeckley, T. R. 1968, MNRAS, 140, 121
Tinbergen, J. 1982, A&A, 105, 53

Uesugi, A., & Fukuda, I. 1982, Revised Catalogue of Stellar Rotational Velocities (Kyoto: Kyoto Univ.)
van Belle, G. T., Dyck, H. M., Benson, J. A., & Lacasse, M. G. 1996, AJ, 112, 2147
van Belle, G. T., Dyck, H. M., Thompson, R. R., Benson, J. A., & Kannappan, S. J. 1997, AJ, 114, 2150
van Belle, G. T., Lane, B. F., Thompson, R. R., & The PTI Collaboration. 1999, AJ, 117, 521
von Zeipel, H. 1924a, MNRAS, 84, 665
———. 1924b, MNRAS, 84, 684
Zahn, J.-P. 1992, A&A, 265, 115